

## RESEARCH ARTICLE

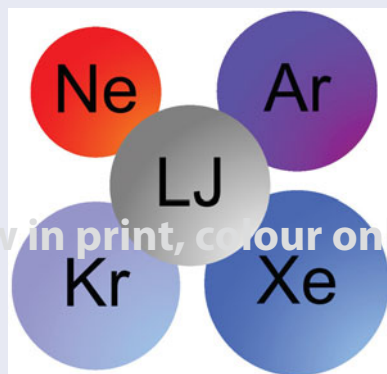
## How well does the Lennard-Jones potential represent the thermodynamic properties of noble gases?

Gábor Rutkai<sup>a</sup>, Monika Thol<sup>b</sup>, Roland Span<sup>b</sup> and Jadran Vrabec<sup>a</sup><sup>a</sup>Lehrstuhl für Thermodynamik und Energietechnik, Universität Paderborn, Paderborn, Germany; <sup>b</sup>Lehrstuhl für Thermodynamik, Ruhr-Universität Bochum, Bochum, Germany**ABSTRACT**

The Lennard-Jones potential as well as its truncated and shifted ( $r_c = 2.5\sigma$ ) variant are applied to the noble gases neon, argon, krypton, and xenon. These models are comprehensively compared with the currently available experimental knowledge in terms of vapour pressure, saturated liquid density, as well as thermodynamic properties from the single phase fluid regions including density, speed of sound, and isobaric heat capacity data. The expectation that these potentials exhibit a more modest performance for neon as compared to argon, krypton, and xenon due to increasing quantum effects does not seem to hold for the investigated properties. On the other hand, the assumption that the truncated and shifted ( $r_c = 2.5\sigma$ ) variant of the Lennard-Jones potential may have shortcomings because the long range interactions are entirely neglected beyond the cut-off radius  $r_c$ , are supported by the present findings for the properties from the single phase fluid regions. For vapour pressure and saturated liquid density such a clear assessment cannot be made.


**ARTICLE HISTORY**Received 30 August 2016  
Accepted 30 September 2016**KEYWORDS**

Neon; argon; krypton; xenon; noble gas; molecular simulation; Lennard-Jones; thermodynamic properties

**Introduction**

All thermodynamic properties can be obtained from molecular simulation on the basis of a molecular force field but the results entirely depend on the underlying molecular model [1]. Such models are necessary because the computation time requirement of the essentially *ab initio* way of determining properties of fluids, other than at low density [2–4], is still too large. After obtaining the charge distribution and geometry of molecular models usually from *ab initio* calculations, their parameters for repulsion and dispersion have to be fitted to macroscopic experimental data. The current trend is to **optimise**

these parameters to a relatively narrow selection of thermodynamic data. Major features of the fluid region, typically vapour pressure and saturated liquid density data from laboratory measurements, are considered in this task because these are usually available in the literature and also because they can be accurately sampled in simulations [5–7]. The most basic assumption of molecular modelling and simulation is that force field models provide meaningful results at state points and for properties that were not considered during their **optimisation**. However, this assumption has rarely been tested in a systematic way. Furthermore, the **optimisation** of the molecular interaction parameters of simple models considering

**CONTACT** Jadran Vrabec ✉ [jadran.vrabec@upb.de](mailto:jadran.vrabec@upb.de)
 Supplemental data for this article can be accessed at <http://dx.doi.org/10.1080/00268976.2016.1246760>.

© 2016 Informa UK Limited, trading as Taylor &amp; Francis Group

a large number and various types of reference data may not provide an overall better solution than that of the relatively narrow selection if the molecular model itself is not flexible enough. In fact, it is very likely that an improvement in one objective cannot be achieved without causing deterioration in others [8]. Nonetheless, recent findings showed that simple molecular models exhibit good agreement with accurate equation of state (EOS) correlations in the temperature and pressure range of industrial relevance for essentially every measurable static thermodynamic property, even if those models were optimised exclusively to a narrow set of vapour pressure and saturated liquid density data. The supplementary material of Ref. [9] presents numerous examples in detail.

An empirical EOS correlation is an explicit relation between state variables and it provides inter- and extrapolation schemes both in states and properties. State-of-the-art empirical EOS [10] are commonly given as an explicit function of a thermodynamic potential,

$$\alpha(T, \rho) = \frac{a(T, \rho)}{RT}, \quad (1)$$

where  $a$  is the molar Helmholtz energy,  $T$  is the temperature,  $\rho = 1/\nu$  is the molar density, and  $R$  is the gas constant. The thermodynamic potential  $\alpha$  is an appropriate choice because its derivatives with respect to its natural variables,  $1/T$  and  $\rho$ , do not involve entropic properties. Independent on the choice of the underlying thermodynamic potential, any static thermodynamic property can be obtained as a combination of its specific partial derivatives with respect to its independent variables by means of simple analytical derivation. Because  $\alpha$  cannot be measured in laboratory, the actual mathematical form that represents  $\alpha$ , along with its parameters, is fitted to its derivatives,

$$\frac{\partial^{m+n}\alpha(1/T, \rho)}{\partial^m(1/T)\partial^n\rho}(1/T)^m\rho^n = A_{mn} = A_{mn}^o + A_{mn}^r. \quad (2)$$

This equation shows that  $A_{mn}$  can be additively decomposed into an ideal (o) and a residual (r) contribution. The ideal contribution is defined as the value of  $A_{mn}$  when no intermolecular interactions are at work. Furthermore,  $A_{mn}^o = 0$  for  $m > 0$  and  $n > 0$ ;  $A_{mn}^o = (-1)^{1+n}$  for  $m = 0$  and  $n > 0$ ;  $A_{mn}^o = A_{mn}^o(T)$  for  $m > 0$  and  $n = 0$  [10]. Naturally, the goal is to consider as many different derivatives in terms of order of differentiation as possible for a given state point during the fit. There are two derivatives ( $A_{01}$ ,  $A_{20}$ ) that are individually accessible via pressure  $p$ , density  $\rho$ , temperature  $T$ , and isochoric heat capacity  $c_v$  measurements. There are two additional derivatives ( $A_{11}$ ,  $A_{02}$ ) that are accessible only

together with  $A_{01}$  and  $A_{20}$  via isobaric heat capacity  $c_p$ , speed of sound  $w$ , or Joule-Thomson coefficient  $\mu$  measurements [10],

$$\frac{p}{\rho RT} = 1 + A_{01}^r, \quad (3)$$

$$\frac{c_v}{R} = -A_{20}^o - A_{20}^r, \quad (4)$$

$$\frac{c_p}{R} = -A_{20}^o - A_{20}^r + \frac{(1 + A_{01}^r - A_{11}^r)^2}{1 + 2A_{01}^r + A_{02}^r}, \quad (5)$$

$$\frac{Mw^2}{RT} = 1 + 2A_{01}^r + A_{02}^r - \frac{(1 + A_{01}^r - A_{11}^r)^2}{A_{20}^o + A_{20}^r}, \quad (6)$$

and

$$\mu\rho R = \frac{-(A_{01}^r + A_{02}^r + A_{11}^r)}{(1 + A_{01}^r - A_{11}^r)^2 - (A_{20}^o + A_{20}^r)(1 + 2A_{01}^r + A_{02}^r)}, \quad (7)$$

where  $M$  is the molar mass. For the noble gases, the ideal contribution  $A_{20}^o$  is  $-3/2$ .

Noble gases, compared to other substances, are well measured. This is particularly true for argon, for which a reference quality EOS is available [11]. Such an EOS represents all reliable experimental data essentially within their uncertainties and it is based on such an amount of excellent data that the EOS can be used to calibrate experimental equipment. The most recent EOS for neon [12], krypton [13], and xenon [13] are also accurate for most technical applications, but they do not fulfil the high standard of reference quality EOS simply because of insufficient experimental data. These EOS are commonly considered as technical references, using a functional form that has been optimised for the representation of properties at pressures of up to 100 MPa. Extrapolation to higher pressure is possible, but no attempts were made to accurately represent there.

Molecular simulation can provide any  $A_{mn}^r$  directly from a single molecular simulation run per state point with the formalism proposed by Lustig [14,15]. Moreover, molecular simulation is not limited by extreme conditions (temperature or pressure) or the nature of the substance. It takes only days to prepare a data-set by molecular simulation that comprises a large quantity of non-redundant thermodynamic information, i.e.  $A_{mn}^r$  data, and covers the entire fluid region [9]. Furthermore, the financial cost of such a data-set is only a tiny fraction of a complete experimental scenario. These data can conveniently be used in EOS correlation [9,16–18] and was recently employed along with non-linear fitting techniques to develop the currently most accurate EOS for the

110 Lennard-Jones (LJ) potential [19] as well as its truncated  
and shifted ( $r_c = 2.5\sigma$ ) variant [20]. The latter two EOS  
will be used for comparison purposes throughout this  
work. A detailed assessment of these correlations with  
115 respect to the underlying simulation data and other avail-  
able EOS [21–23] can be found in Refs. [19,20].

## Lennard-Jones potential

The LJ potential [24,25],

$$u_{\text{LJ}}(r) = 4\varepsilon \left[ \left( \frac{\sigma}{r} \right)^{12} - \left( \frac{\sigma}{r} \right)^6 \right] \quad (8)$$

with its parameters for energy  $\varepsilon$  and size  $\sigma$  describes the  
interaction energy between two spherical particles at a  
120 distance  $r$  from each other. It represents repulsion and  
dispersive attraction. In itself, it is well suited to model  
the interactions between noble gas or methane molecules  
[26]. The truncated and shifted Lennard-Jones (LJTS)  
potential [1],

$$u_{\text{LJTS}}(r) = \begin{cases} u_{\text{LJ}}(r) - u_{\text{LJ}}(r = r_c) & \text{for } r \leq r_c \\ 0 & \text{for } r > r_c \end{cases} \quad (9)$$

125 is a common modification that artificially removes inter-  
actions beyond the cut-off radius  $r_c$ . This truncation  
avoids the calculation of long-range corrections [1],  
which may be problematic or numerically costly in inho-  
mogeneous systems, while the shift with  $u_{\text{LJ}}(r = r_c)$   
130 enforces a decay to zero that is expected for the inter-  
molecular interaction energy. The LJTS potential is also  
considered to be sufficiently realistic to represent noble  
gases [27], but it differs significantly from the LJ poten-  
tial in terms of its thermodynamic properties (e.g. there  
135 is 20% difference in the critical temperature for the same  
 $\varepsilon$  parameter). The LJ potential is undisputedly the most  
frequently applied model in molecular simulation history  
because it was, and most likely still is, the best trade-off  
140 between computational cost, accuracy, and compatibil-  
ity. More sophisticated potentials are available, e.g. with  
adjustable exponent for the repulsive interaction [28] or  
the explicit consideration of three-body interactions [29].  
Due to being physically more reasonable and having more  
adjustable parameters, these potentials must provide  
145 better agreement with experimental data. Nonetheless,  
they certainly involve more computation time. Further-  
more, their application to inhomogeneous systems or for  
the calculation of complex properties may be difficult,  
and compatible molecular models have to be developed  
150 for all components in mixture simulations.

It is clear that multicriteria **optimisation** of simple  
molecular models with few parameters most likely means  
making concessions. As long as a potential does not

describe molecular interactions accurately enough to  
derive all macroscopic thermodynamic properties with  
155 equally high accuracy, an improvement in the representa-  
tion of some thermodynamic property inevitably causes  
deterioration in the representation of others. It is pos-  
sible to map the set of best compromises if sufficient  
160 experimental reference data are available for multicri-  
teria **optimisation** [8]. The data availability in the liter-  
ature is unfortunately poor to very poor for most flu-  
ids. Therefore, we assume here the most likely scenario,  
i.e. that vapour pressure  $p_v$  and saturated liquid density  
165  $\rho'$  data are the only experimental data available for the  
**optimisation** of the interaction potential parameters (in  
this case  $\varepsilon$  and  $\sigma$ ). Therefore, the values of these param-  
eters for neon (LJ), argon (LJ and LJTS), and krypton (LJ  
and LJTS) were essentially taken from works [27,30] for  
170 which the **optimisation** was based on  $p_v$  and  $\rho'$ . However,  
the parameters for each noble gas and potential were also  
determined here with a simple algorithm: Based on the  
fundamental EOS, the energy  $\varepsilon$  and size  $\sigma$  parameters of  
the fundamental equations of state of the two **LJ** poten-  
175 tials [19,20] were adjusted to the most accurate experi-  
mental data for the values of the critical temperature  $T_c$   
and density  $\rho_c$  according to  $T_c = T_c^* \cdot (\varepsilon/k_B)$  and  $\rho_c =$   
 $\rho_c^* / \sigma^3$ , where  $T_c^*$  and  $\rho_c^*$  are the reduced critical data  
of the two potentials which are constants. For neon (LJ),  
180 argon (LJ and LJTS), and krypton (LJ and LJTS), this pro-  
cedure yielded the same results as found in the literature  
[8,27,30]. For xenon, differences were observed due to a  
likely typo in Refs. [27,30]: Since the overall representa-  
tion of the literature data with the new xenon paramet-  
185 ers was much better than with the literature values, they were  
adopted for the following investigations. The parameters  
values are **summarised** in Table 1.

## Results

The available quality and quantity of experimental data  
in the literature made fundamental EOS correlations for  
190

**Table 1.** Parameter values for energy  $\varepsilon$  and size  $\sigma$  used in  
this work, where  $k_B$  is the Boltzmann constant. Values were  
determined with an algorithm described in the text.

|                          | LJ     | LJTS   |
|--------------------------|--------|--------|
| Ne                       |        |        |
| $\varepsilon/k_B$ (K)    | 33.921 | 39.83  |
| $\sigma$ ( $10^{-10}$ m) | 2.801  | 2.800  |
| Ar                       |        |        |
| $\varepsilon/k_B$ (K)    | 116.79 | 137.90 |
| $\sigma$ ( $10^{-10}$ m) | 3.3952 | 3.3916 |
| Kr                       |        |        |
| $\varepsilon/k_B$ (K)    | 162.58 | 191.52 |
| $\sigma$ ( $10^{-10}$ m) | 3.6274 | 3.6233 |
| Xe                       |        |        |
| $\varepsilon/k_B$ (K)    | 226.14 | 274.86 |
| $\sigma$ ( $10^{-10}$ m) | 3.949  | 3.946  |

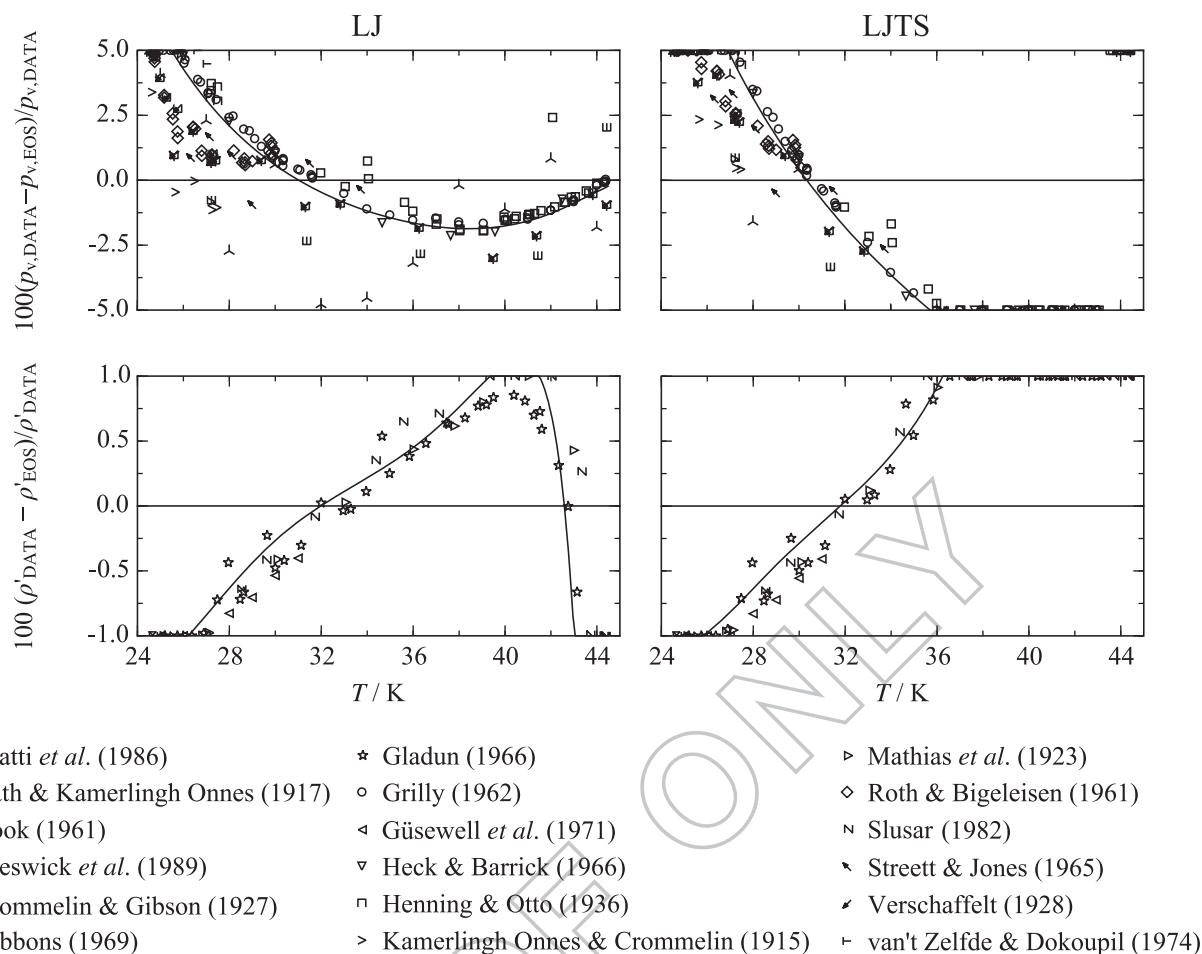


**Figure 1.** Relative deviations for the vapour pressure  $p_v$  and saturated liquid density  $\rho'$  between the EOS for LJ [19] or LJTS [20] (baselines) and experimental data (represented by various symbols) for neon. The references for experimental data are given in the supplementary material. The solid line denotes the EOS of Katti *et al.* [12].

**Table 2.** Average deviations (low density  $\langle LD \rangle$ , medium density  $\langle MD \rangle$  and high density  $\langle HD \rangle$ ) calculated by  $\langle 100 \bullet (X_{\text{Ref}} - X_{\text{LJ,LJTS}})/X_{\text{Ref}} \rangle$  for the property  $X$  (density  $\rho$ , pressure  $p$ , or speed of sound  $w$ ) at single phase fluid state points.  $X_{\text{Ref}}$  represents the EOS of either Katti *et al.* [12] (neon), Tegeler *et al.* [11] (argon), or Lemmon and Span [13] (krypton and xenon) and  $X_{\text{LJ,LJTS}}$  represents the value from the EOS for LJ [19] or LJTS [20]. For each noble gas, the average  $\langle \bullet \rangle$  is based on 740 state points along 37 isotherms: 17 from the interval  $0.66 \leq T/T_c \leq 0.98$  (increment 0.02) and 20 from the interval  $1.1 \leq T/T_c \leq 3.0$  (increment 0.1). Below the critical temperature  $T_c$ , 10 densities were specified between  $\rho/\rho_c = 0.001$  and  $\rho''/\rho_c$  (increment  $(\rho''/\rho_c - 0.001)/10$ ) and 10 densities between  $\rho'/\rho_c$  and  $\rho/\rho_c = 2.55$  (increment  $(2.55 - \rho'/\rho_c)/10$ ), where  $\rho''$  is the saturated vapour density and  $\rho'$  the saturated liquid density. Twenty densities were specified above  $T_c$  between  $\rho/\rho_c = 0.001$  and 2.55 (increment  $(2.55 - 0.001)/20$ ). The difference between the ideal pressure and that of the respective noble gas is around 0.3% at  $\rho/\rho_c = 0.001$  and  $T/T_c = 0.6$ .  $T_t/T_c \approx 0.55$  and  $\rho_t/\rho_c \approx 2.6$  for the triple point ( $T_t, \rho_t$ ). LD:  $\rho/\rho_c < 0.6$ ; MD:  $0.6 \leq \rho/\rho_c \leq 1.5$ ; HD:  $\rho/\rho_c > 1.5$ . Lowest values in each subcolumn (LJ or LJTS) are shaded.

|      |    | $\rho$ |      |      | $p$  |      |      | $w$  |      |      |
|------|----|--------|------|------|------|------|------|------|------|------|
|      |    | LD     | MD   | HD   | LD   | MD   | HD   | LD   | MD   | HD   |
| LJ   | Ne | 0.72   | 1.27 | 0.63 | 0.55 | 1.68 | 4.36 | 0.46 | 1.80 | 1.76 |
|      | Ar | 1.01   | 0.57 | 0.29 | 0.74 | 0.63 | 2.31 | 0.56 | 1.61 | 1.47 |
|      | Kr | 1.14   | 0.88 | 0.33 | 0.85 | 1.04 | 4.48 | 0.91 | 2.31 | 1.94 |
|      | Xe | 1.08   | 0.93 | 0.38 | 0.83 | 1.10 | 3.15 | 0.95 | 2.45 | 2.18 |
| LJTS | Ne | 0.59   | 3.46 | 1.55 | 0.51 | 4.51 | 8.52 | 0.42 | 2.50 | 3.21 |
|      | Ar | 0.56   | 2.07 | 0.78 | 0.46 | 2.57 | 3.49 | 0.48 | 2.02 | 3.68 |
|      | Kr | 0.79   | 2.56 | 0.68 | 0.64 | 3.18 | 4.37 | 0.86 | 2.78 | 3.06 |
|      | Xe | 0.69   | 2.40 | 1.11 | 0.59 | 2.99 | 3.64 | 0.92 | 2.93 | 3.41 |

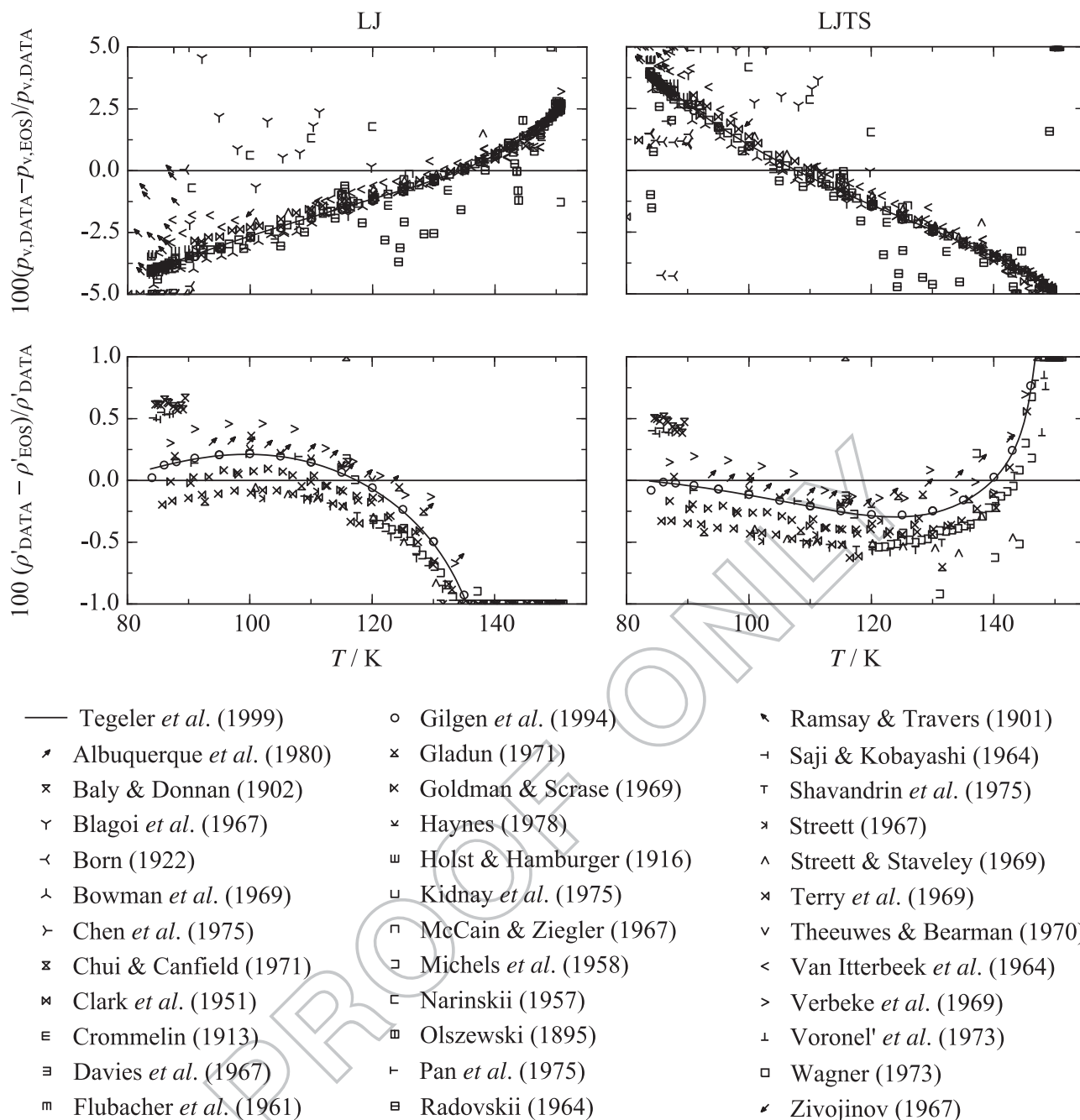


**Figure 2.** Relative deviations for the vapour pressure  $p_v$  and saturated liquid density  $\rho'$  between the EOS for LJ [19] or LJTS [20] (baselines) and experimental data (represented by various symbols) for argon. The references for experimental data are given in the supplementary material. The solid line denotes the EOS of Tegeler *et al.* [11].

noble gases sensible [11–13]. Their underlying data sets consist mainly of vapour pressure, saturated liquid density, along with  $p\rho T$  and speed of sound data from the single phase fluid regions. A sufficient amount of isobaric heat capacity data is available only for argon to make comparisons meaningful. During the construction of a reference EOS, the literature data are carefully screened and a considerable part of it is discarded. In this work,

we use the experimental data that were found trustworthy based on previous efforts [11–13]. Fundamental EOS development also enables assessing the available data in terms of uncertainty beyond the standard uncertainty estimation of the individual measurements. In fact, EOS are often more precise than the individual measurements. One obvious reason behind this lies in the statistical benefit of being able to compare results from different



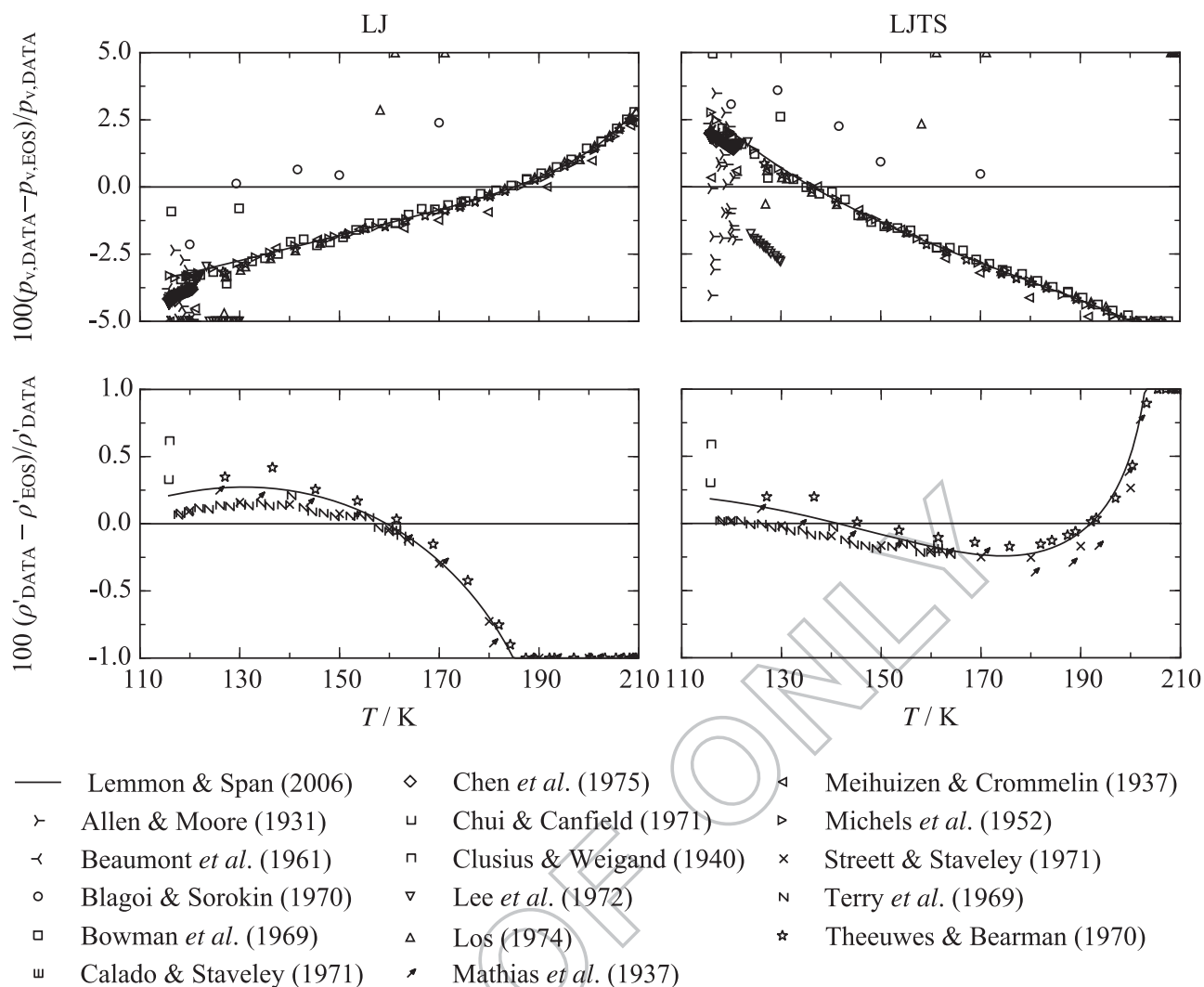


**Figure 3.** Relative deviations for the vapour pressure  $p_v$  and saturated liquid density  $\rho'$  between the EOS for LJ [19] or LJTS [20] (baselines) and experimental data (represented by various symbols) for krypton. The references for experimental data are given in the supplementary material. The solid line denotes the EOS of Lemmon and Span [13].

laboratories. The more data available, the clearer the assessment about the general uncertainty of experimental data becomes. The other, and stronger, reason is that thermodynamic consistency is a built-in feature of fundamental EOS because they rigorously connect all thermodynamic properties through mathematical transformations. Inconsistencies in the underlying data set are thus usually directly detectable. According to the reference quality EOS for argon [11], the scatter of the experimental data compared to the EOS (at specified  $p$  and  $T$ ) considering the entire data set is usually not larger than 0.5% for density, 1% for the speed of sound, and 10% for the isobaric heat capacity (see below). Deviation of the EOS from the most accurate density and speed of sound measurements, which determined the accuracy of the correlation, is below 0.02% for both properties.

The LJ and LJTS EOS used in this work represent most of the molecular simulation data within 1% for density, 5% for the speed of sound, and 10% for the isobaric heat capacity. The relative differences between various experimental data and the underlying EOS are shown in Figures 1–14. Deviations tend to increase closer to the critical point (approximately 44.5 K and 2.68 MPa for neon [12], 150.7 K and 4.86 MPa for argon [11], 209.5 K and 5.53 MPa for krypton, and 289.7 K and 5.84 MPa for xenon [13]).

Due to increasing quantum effects, the expectation is that the LJ and LJTS potentials exhibit a more modest performance for neon as compared to argon, krypton, and xenon. Furthermore, one would also expect that the LJTS potential may face problems due to entirely neglecting long range interactions beyond  $r_c = 2.5\sigma$ .

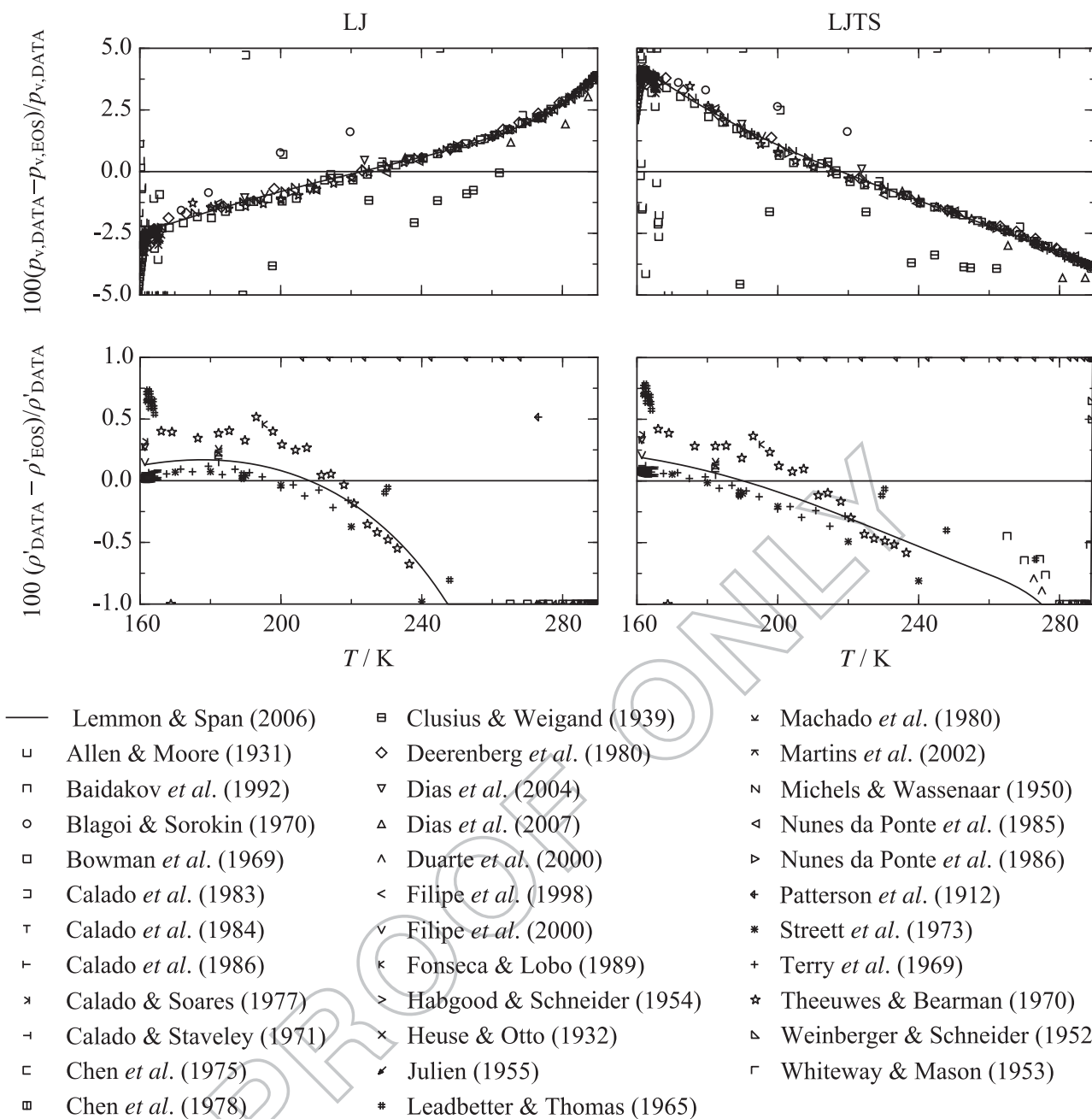
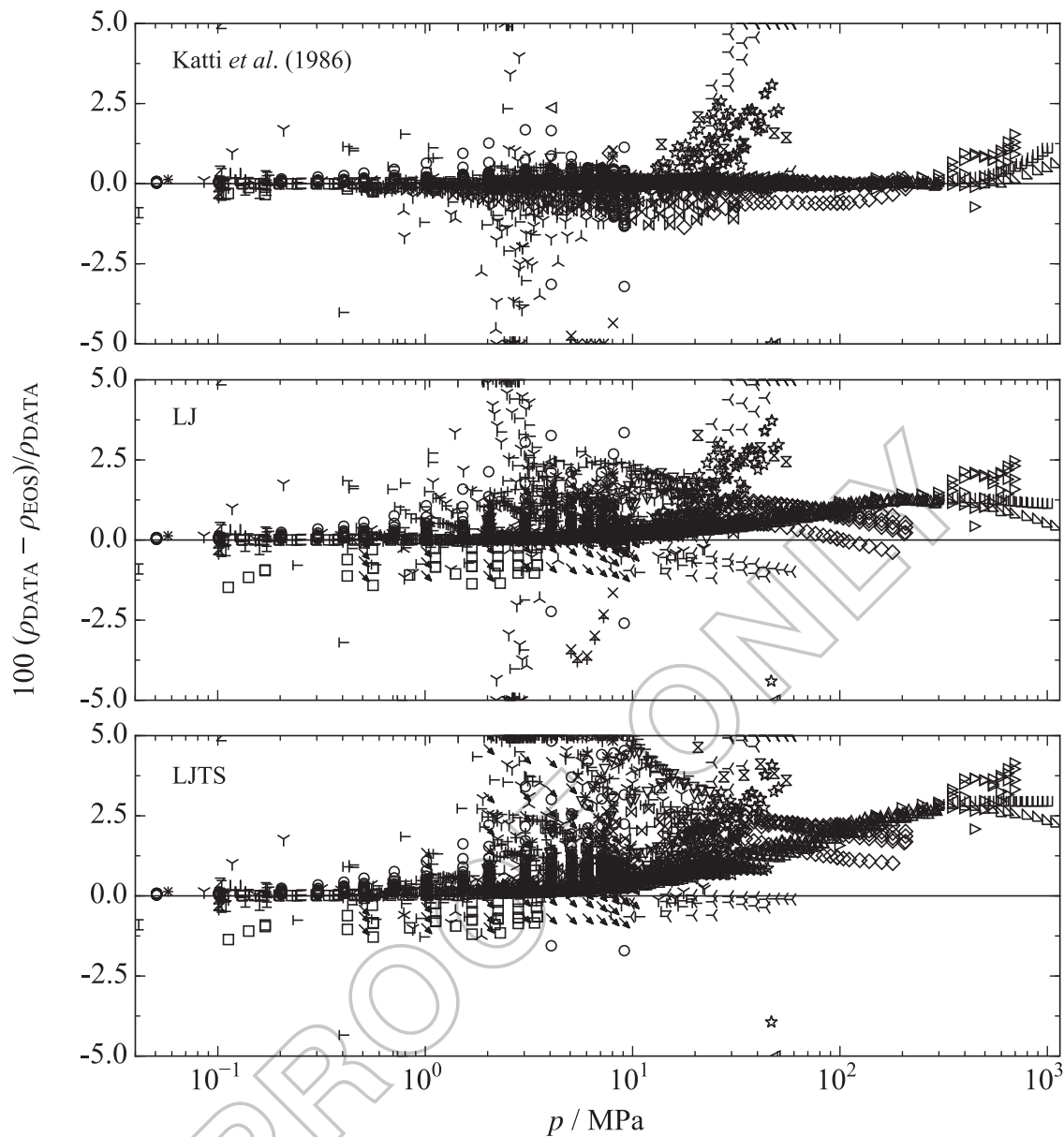


**Figure 4.** Relative deviations for the vapour pressure  $p_v$  and saturated liquid density  $\rho'$  between the EOS for LJ [19] or LJTS [20] (baselines) and experimental data (represented by various symbols) for xenon. The references for experimental data are given in the supplementary material. The solid line denotes the EOS of Lemmon and Span [13].

240 The latter statement seems to hold at the investigated single phase fluid regions for the density (Figures 5–8 and 14), speed of sound (Figures 9–12), and isobaric heat capacity (Figure 13). Namely, the experimental data are distributed more evenly with respect to the negative and positive directions for the LJ potential, while the distribution for the LJTS potential rather shows a distinct offset to the experimental data (positive for density, negative for speed of sound). For vapour pressure  $p_v$  and

saturated liquid density  $\rho'$ , such a clear assessment cannot be made: LJ and LJTS are relatively similar for  $p_v$  and  $\rho'$  in terms of overall performance (Figures 1–4). The only exception is neon, for which the LJ potential clearly shows a better agreement with experimental  $p_v$  and  $\rho'$  data than its truncated and shifted variant (Figure 1). Furthermore, a comparison of this figure with the following three somewhat justifies the expectation of a presumably poorer representation quality for neon than for the



- |                                       |                                     |                                   |
|---------------------------------------|-------------------------------------|-----------------------------------|
| + Crommelin (1918)                    | * Kestin & Leidenfrost (1959)       | ☆ Rabinovich <i>et al.</i> (1970) |
| ⊢ DiPippo <i>et al.</i> (1968)        | z Kestin & Nagashima (1964)         | γ Scott (1967)                    |
| ⊣ DiPippo & Kestin (1968)             | ⊠ Kestin & Whitelaw (1963)          | ○ Stewart & Johnson (1961)        |
| ♣ Evers <i>et al.</i> (2002)          | ⊡ Kortbeek <i>et al.</i> (1988)     | ⊗ Streett (1968)                  |
| ⋈ Flynn <i>et al.</i> (1963)          | ↖ Lippold (1969)                    | ◇ Streett (1971)                  |
| ⊢ Gibbons (1969)                      | ▷ Maslennikova <i>et al.</i> (1976) | □ Streett (1973)                  |
| ↘ Gladun (1967)                       | △ Michels <i>et al.</i> (1960)      | ⊗ Sullivan & Sonntag (1967)       |
| ♣ Holborn & Otto (1924)               | ◁ Michels & Gibson (1928)           | ▵ Vidal & Lallemand (1975)        |
| > Holborn & Otto (1926)               | ⋈ Onosovskii (1975)                 | ⊞ Vogl & Hall (1972)              |
| × Kamerlingh Onnes & Crommelin (1915) | ▽ Osnovskii & Moroz (1970)          |                                   |

**Figure 5.** Relative deviations for the single phase density  $\rho$  between three EOS (LJ [19], LJTS [20], or the EOS of Katti *et al.* [12], baselines) and experimental data (represented by various symbols) for neon. The references for experimental data are given in the supplementary material.



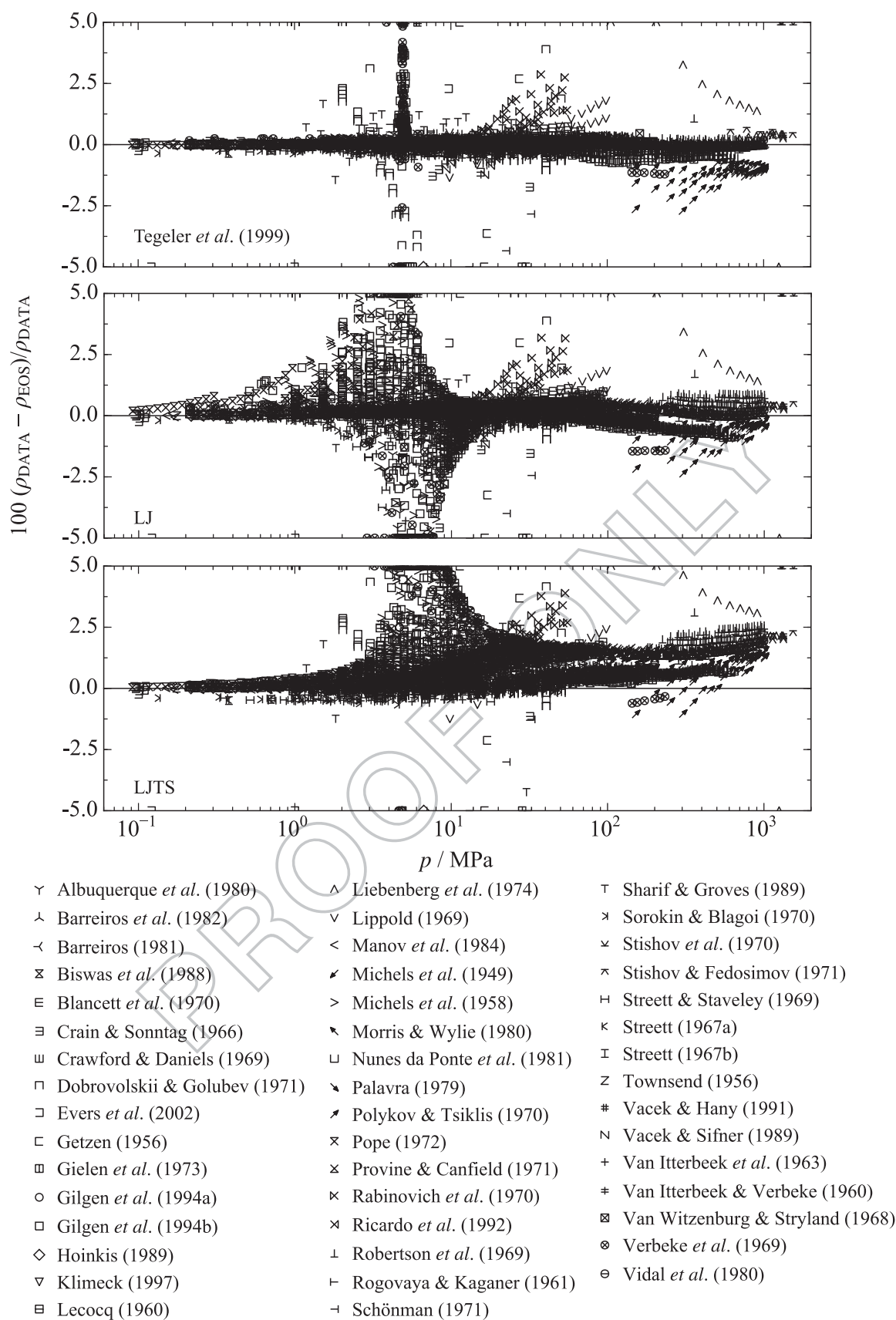


**Figure 6.** Relative deviations for the single phase density  $\rho$  between three EOS (LJ [19], LJTS [20], or the EOS of Tegeler *et al.* [11], baselines) and experimental data (represented by various symbols) for argon. The references for experimental data are given in the supplementary material.

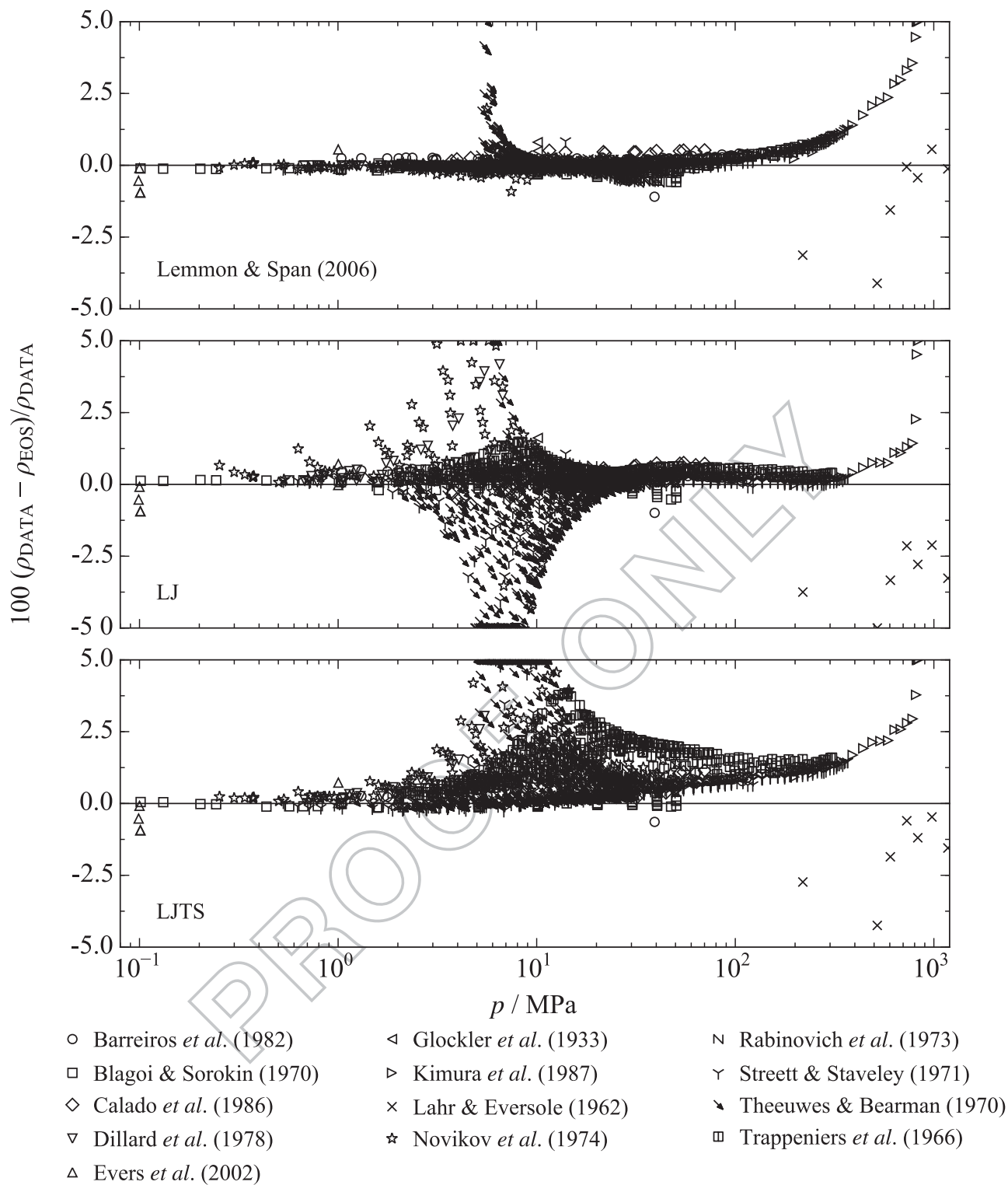


**Figure 7.** Relative deviations for the single phase density  $\rho$  between three EOS (LJ [19], LJTS [20], or the EOS of Lemmon and Span [13], baselines) and experimental data (represented by various symbols) for krypton. The references for experimental data are given in the supplementary material.

other noble gases, but only for the LJTS potential. Interestingly, the comparisons for the properties from the single phase fluid regions do not support this expectation:

According to the density and speed of sound deviation 260 plots (Figures 5–12 and 14), the quality of representation is roughly the same for neon as for argon, krypton,

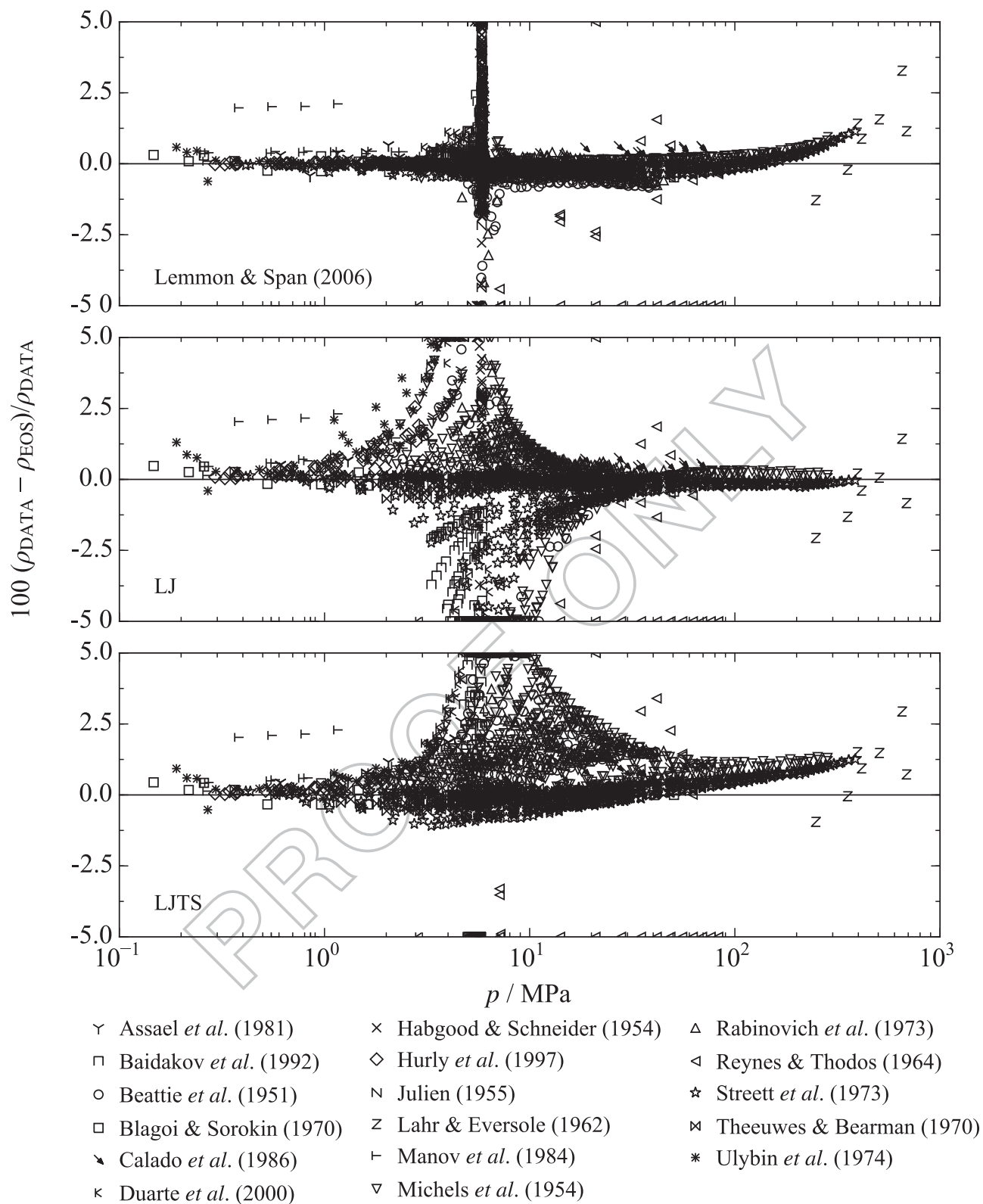


**Figure 8.** Relative deviations for the single phase density  $\rho$  between three EOS (LJ [19], LJTS [20], or the EOS of Lemmon and Span [13], baselines) and experimental data (represented by various symbols) for xenon. The references for experimental data are given in the supplementary material.

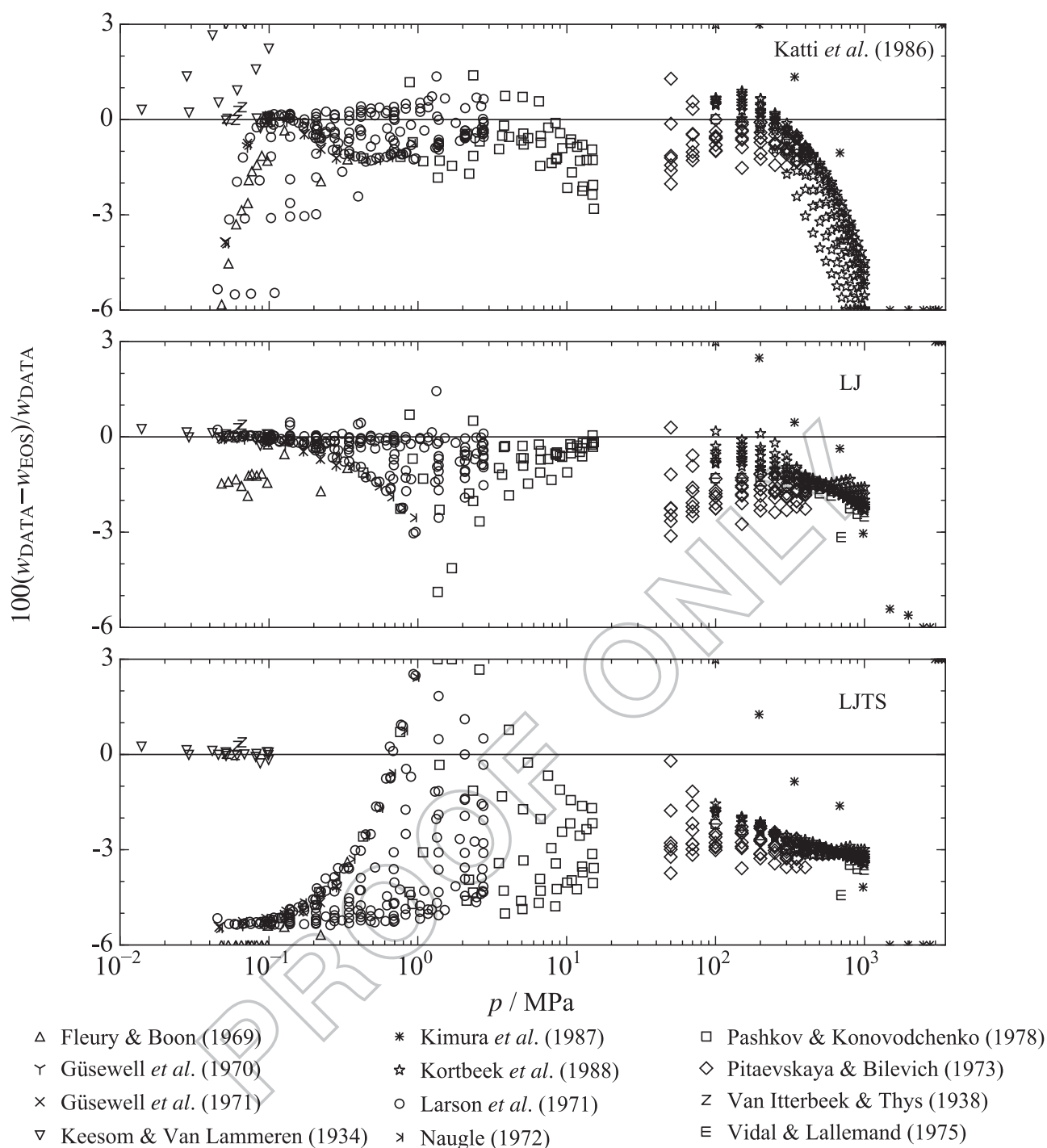
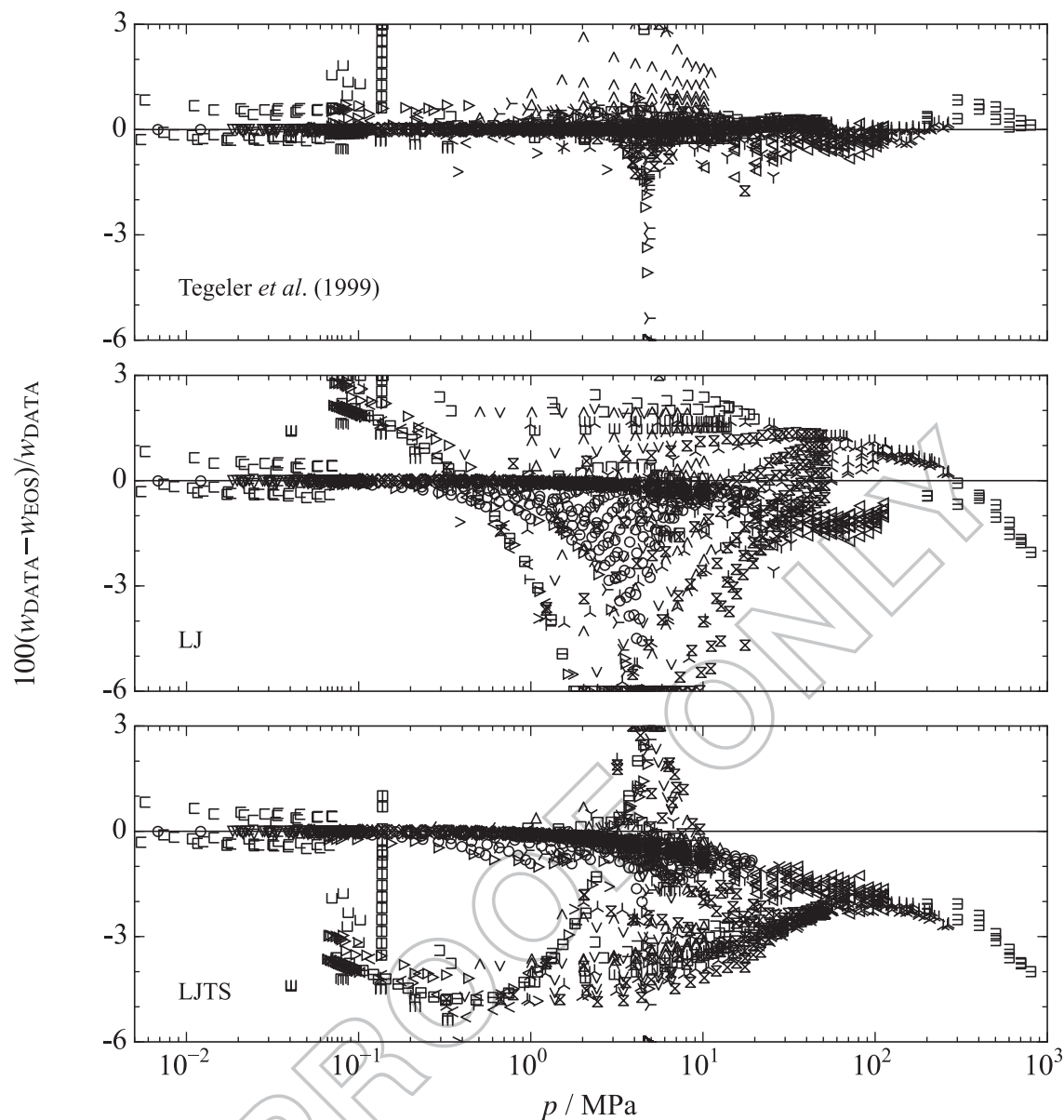


**Figure 9.** Relative deviations for the single phase speed of sound  $w$  between three EOS (LJ [19], LJTS [20], or the EOS of Katti *et al.* [12], baselines) and experimental data (represented by various symbols) for neon. The references for experimental data are given in the supplementary material.

and xenon for the same potential. The numerical data of Table 2 support these findings. In general, the average deviations are not worse for neon as compared to the other noble gases, whereas the overall representation is best for argon. Again, the LJ potential, all in all, shows

better agreement than the LJTS potential. It was expected that the accuracy of these potentials does not reach the level that of the most accurate experimental data and thus the reference quality EOS of Tegeler *et al.* [11] (e.g. below 0.02% for the density, cf. Figure 14). Nonetheless,



- |                                       |                                 |                                      |
|---------------------------------------|---------------------------------|--------------------------------------|
| ⊖ Aziz <i>et al.</i> (1967)           | ⊓ Fleury & Boon (1969)          | ⊘ Susekov (1972)                     |
| ⊐ Beckermann & Kohler (1993)          | ☆ Hurly <i>et al.</i> (2003)    | ⊗ Thoen <i>et al.</i> (1969)         |
| < Blagoi <i>et al.</i> (1967)         | ⊚ Kachanov <i>et al.</i> (1983) | ⊢ Thoen <i>et al.</i> (1971)         |
| > Blagoi <i>et al.</i> (1968)         | △ Lacam & Noury (1953)          | ⊞ Van Dael <i>et al.</i> (1966)      |
| ∨ Bowman <i>et al.</i> (1968)         | ◁ Lacam (1956)                  | ⊠ Van Itterbeek <i>et al.</i> (1959) |
| ◇ Boyes (1992)                        | ⊗ Lim & Aziz (1967)             | ⊐ Van Itterbeek <i>et al.</i> (1969) |
| ^ Carome <i>et al.</i> (1968)         | ▷ Radovskii (1963)              | ⊓ Van Itterbeek & Van Dael (1961)    |
| ⊓ Dobbs & Finegold (1960)             | ∇ Sharif & Groves (1989)        | ⊐ Van Itterbeek & Van Paemel (1938)  |
| ○ Estrada-Alexanders & Trusler (1995) | ∧ Streett & Constantino (1974)  | ⊐ Van Itterbeek & Verhaegen (1949)   |
| ∇ Ewing <i>et al.</i> (1985)          |                                 |                                      |

**Figure 10.** Relative deviations for the single phase speed of sound  $w$  between three EOS (LJ [19], LJTS [20], or the EOS of Tegeler *et al.* [11], baselines) and experimental data (represented by various symbols) for argon. The references for experimental data are given in the supplementary material.



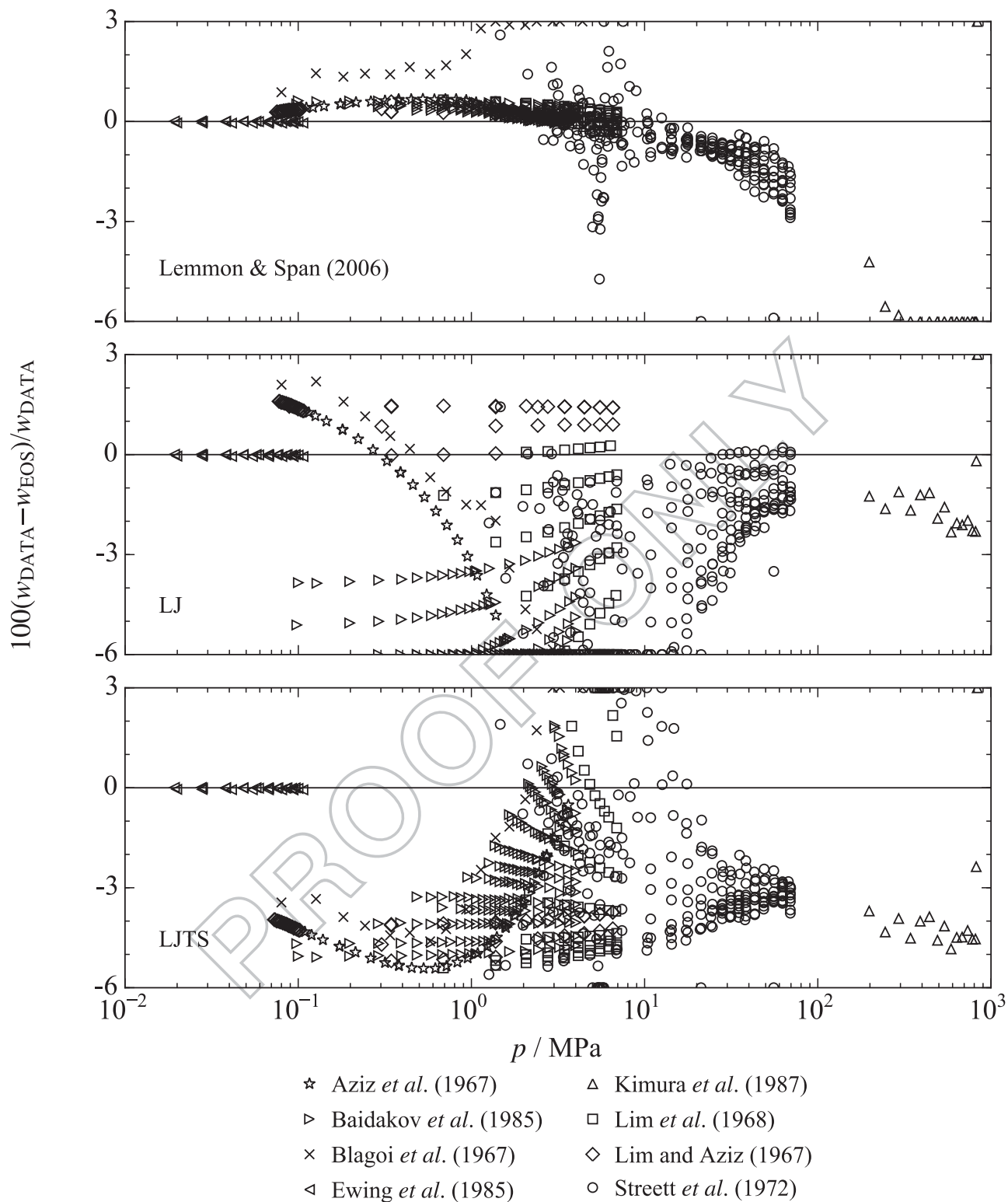


**Figure 11.** Relative deviations for the single phase speed of sound  $w$  between three EOS (LJ [19], LJTS [20], or the EOS of Lemmon and Span [13], baselines) and experimental data (represented by various symbols) for krypton. The references for experimental data are given in the supplementary material.

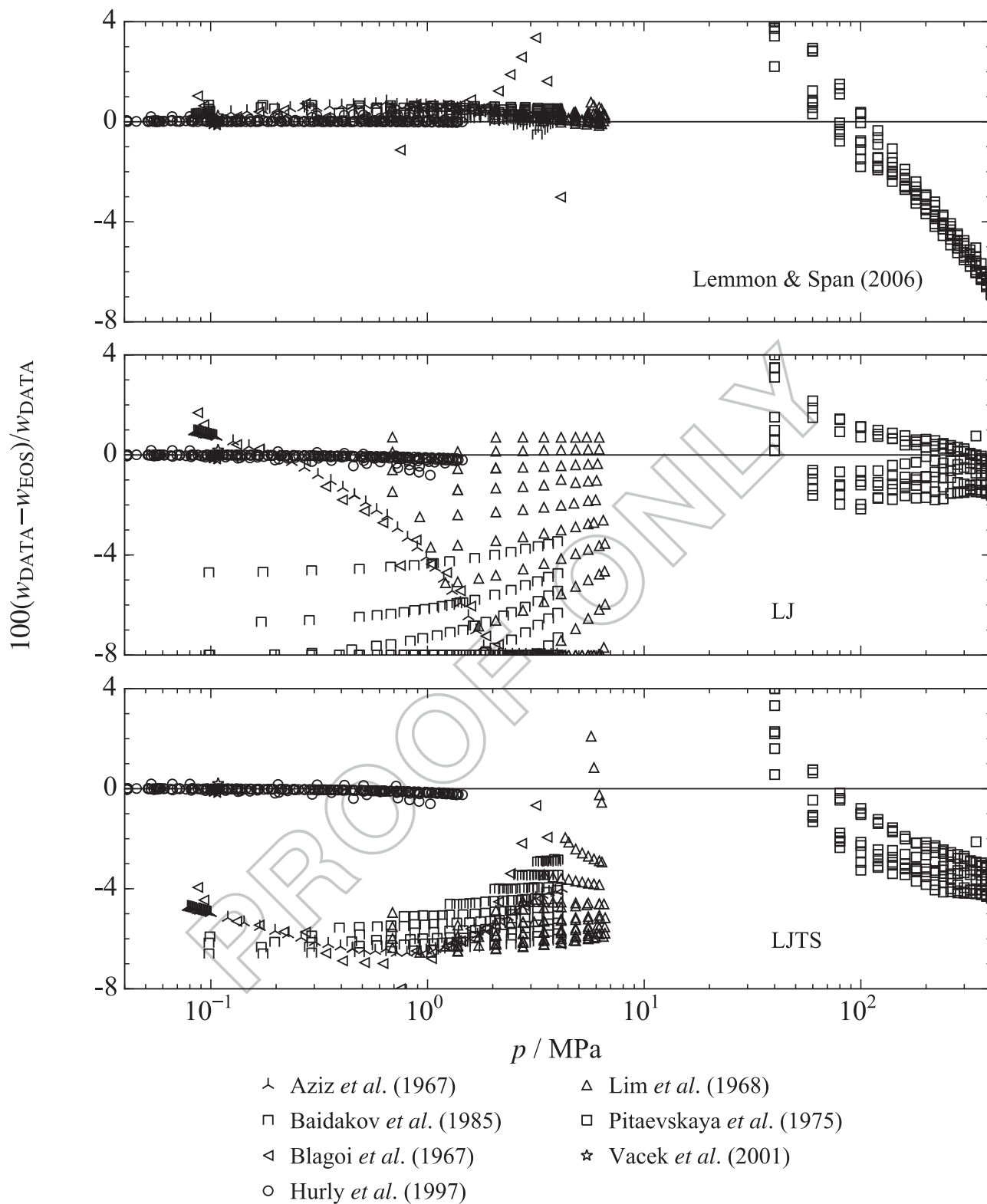


**Figure 12.** Relative deviations for the single phase speed of sound  $w$  between three EOS (LJ [19], LJTS [20], or the EOS of Lemmon and Span [13], baselines) and experimental data (represented by various symbols) for xenon. The references for experimental data are given in the supplementary material.

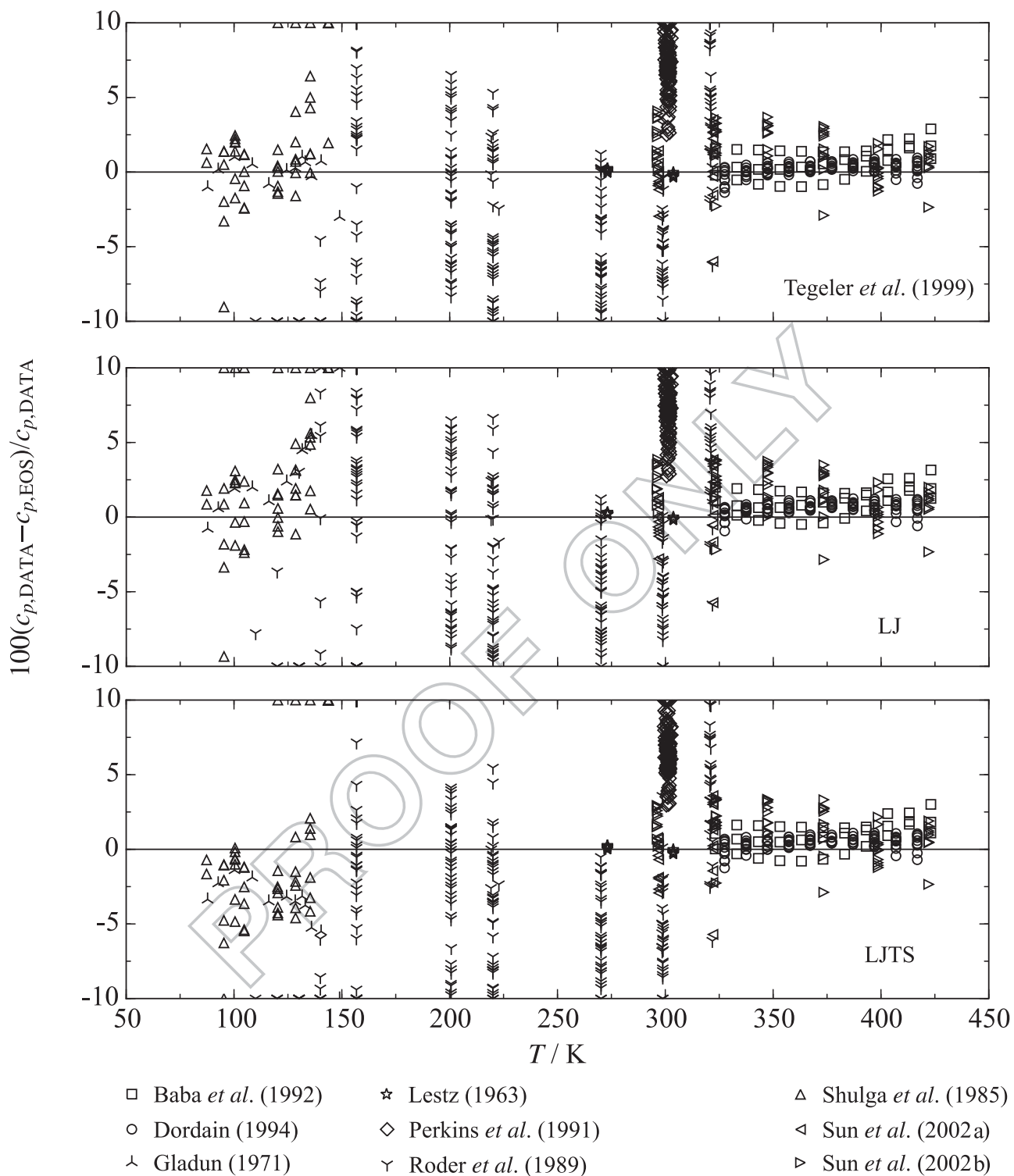


**Figure 13.** Relative deviations for the single isobaric heat capacity  $c_p$  between three EOS (LJ [19], LJTS [20], or the EOS of Tegeler *et al.* [11], baselines) and experimental data (represented by the various symbols) for argon. The references for experimental data are given in the supplementary material.

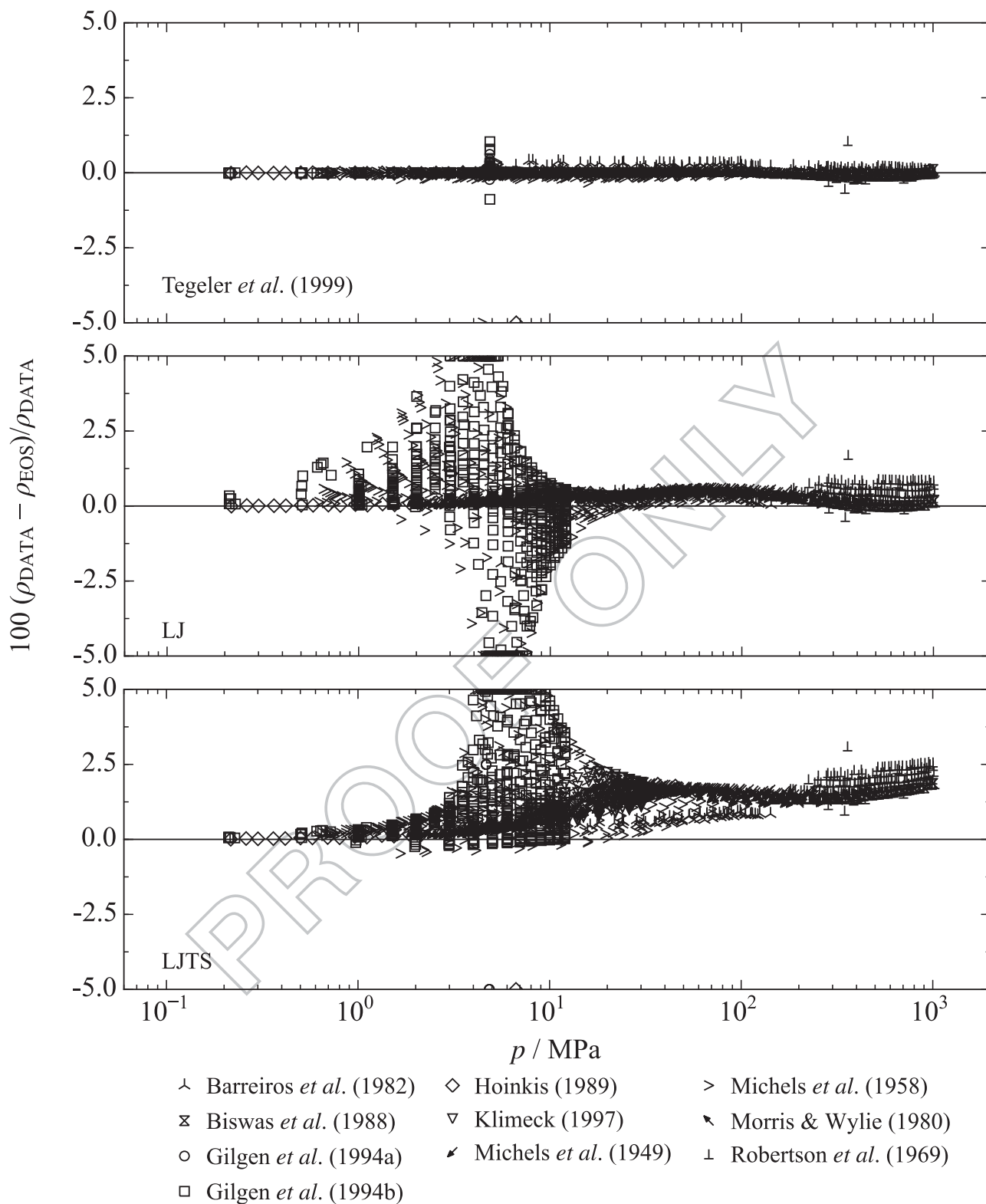


**Figure 14.** Relative deviations for the single phase density  $\rho$  between three EOS (LJ [19], LJTS [20], or the EOS of Tegeler *et al.* [11], baselines) and the most accurate experimental data (represented by various symbols) for argon. The references for experimental data are given in the supplementary material.

the overall agreement with the EOS of Katti *et al.* [12], Tegeler *et al.* [11], and Lemmon and Span [13] is surprisingly good for both the LJ and the LJTS potentials.

## Acknowledgments

The authors gratefully acknowledge financial support by Deutsche Forschungsgemeinschaft under grant Nos. VR6/4-2 and SP507/7-2. The simulations were carried out on the Hazel Hen cluster at the High Performance Computing Center Stuttgart (HLRS) and on the OCuLUS cluster of the Paderborn Center for Parallel Computing (PC<sup>2</sup>).

## Disclosure statement

No potential conflict of interest was reported by the authors.

## Funding

The authors gratefully acknowledge financial support by Deutsche Forschungsgemeinschaft under grant Nos. VR6/4-2 and SP507/7-2.

## References

- [1] D. Frenkel and B. Smit, *Understanding Molecular Simulation. From Algorithms to Applications*, 2nd ed. (Academic Press, Elsevier, San Diego, CA, 2002).
- [2] E. Bich, R. Hellmann, and E. Vogel, *Mol. Phys.* **105**, 3035 (2007).
- [3] E. Bich, R. Hellmann, and E. Vogel, *Mol. Phys.* **106**, 813 (2008).
- [4] E. Vogel, B. Jäger, R. Hellmann, and E. Bich, *Mol. Phys.* **108**, 3335 (2010).
- [5] A. Lotfi, J. Vrabec, and J. Fischer, *Mol. Phys.* **76**, 1319 (1992).
- [6] I. Szalai, J. Liszi, and D. Boda, *Chem. Phys. Lett.* **246**, 214 (1995).
- [7] J. Vrabec and H. Hasse, *Mol. Phys.* **100**, 3375 (2002).
- [8] K. Stöbener, P. Klein, S. Reiser, M. Horsch, K.-H. Küfer, and H. Hasse, *Fluid Phase Equilib.* **373**, 100 (2014).
- [9] G. Rutkai, M. Thol, R. Lustig, R. Span, and J. Vrabec, *J. Chem. Phys.* **139**, 041102 (2013).
- [10] R. Span, *Multiparameter Equations of State. An Accurate Source of Thermodynamic Property Data* (Springer, Berlin, 2000).
- [11] C. Tegeler, R. Span, and W. Wagner, *J. Phys. Chem. Ref. Data.* **28**, 779 (1999).
- [12] R. Katti, R.T. Jacobsen, R.B. Stewart, and M. Jahangiri, in *Advances in Cryogenic Engineering*, edited by R.W. Fast (Springer, Boston, MA, 1986).
- [13] E.W. Lemmon and R. Span, *J. Chem. Eng. Data.* **51**, 785 (2006).
- [14] R. Lustig, *Mol. Sim.* **37**, 457 (2011).
- [15] R. Lustig, *Mol. Phys.* **110**, 3041 (2012).
- [16] M. Thol, G. Rutkai, A. Köster, M. Kortmann, R. Span, and J. Vrabec, *Chem. Eng. Sci.* **121**, 87 (2015); **134**, 887 (2015).
- [17] M. Thol, F.H. Dubberke, G. Rutkai, T. Windmann, A. Köster, R. Span, and J. Vrabec, *Fluid Phase Equilib.* **418**, 133 (2016).
- [18] M. Thol, G. Rutkai, A. Köster, F.H. Dubberke, T. Windmann, R. Span, and J. Vrabec, *J. Chem. Eng. Data.* **61**, 2580 (2016).
- [19] M. Thol, G. Rutkai, A. Köster, R. Span, J. Vrabec, and R. Lustig, *J. Phys. Chem. Ref. Data.* **45**, 023101 (2016).
- [20] M. Thol, G. Rutkai, R. Span, J. Vrabec, and R. Lustig, *Int. J. Thermophys.* **36**, 25 (2015).
- [21] J.K. Johnson, J.A. Zollweg, and K.E. Gubbins, *Mol. Phys.* **78**, 591 (1993).
- [22] M. Mecke, A. Müller, J. Winkelmann, J. Vrabec, J. Fischer, R. Span, and W. Wagner, *Int. J. Thermophys.* **17**, 391 (1996); **19**, 1493 (1998).
- [23] J. Kolafa and I. Nezbeda, *Fluid Phase Equilib.* **100**, 1 (1994).
- [24] J.E. Jones, *Proc. R. Soc. A.* **106**, 441 (1924).
- [25] J.E. Jones, *Proc. R. Soc. A.* **106**, 463 (1924).
- [26] B. Saager and J. Fischer, *Fluid Phase Equilib.* **57**, 35 (1990).
- [27] J. Vrabec, G.K. Kedia, G. Fuchs, and H. Hasse, *Mol. Phys.* **104**, 1509 (2006).
- [28] J.R. Mick, M. Soroush Barhaghi, B. Jackman, K. Rushaidat, L. Schwiebert, and J.J. Potoff, *J. Chem. Phys.* **143**, 114504 (2015).
- [29] F. del Río, E. Díaz-Herrera, O. Guzmán, J.A. Moreno-Razo, and J.E. Ramos, *J. Chem. Phys.* **139**, 184503 (2013).
- [30] J. Vrabec, J. Stoll, and H. Hasse, *J. Phys. Chem. B.* **105**, 12126 (2001).